Available online at www.sciencedirect.com
SCIENCE DIRECT®
Thermochimica Acta 403 (2003) 115–127
thermochimica acta
www.elsevier.com/locate/tca

Microthermal analysis of rubber-polyaniline core-shell microparticles using frequency-dependent thermal responses

Changshu Kuo [a,*], Chien-Chung Chen [b], William Bannister [b]

[a] *Department of Plastics Engineering, University of Massachusetts Lowell, 1 University Avenue, Lowell, MA 01854, USA*
[b] *Department of Chemistry, University of Massachusetts Lowell, 1 University Avenue, Lowell, MA 01854, USA*

Received 2 October 2002; received in revised form 5 February 2003; accepted 6 February 2003

Abstract

Alternating current (ac) thermal microscopy and microthermal analysis have been utilized for the investigation in the surface thermal conductivity imaging and local thermal analysis (LTA) of polybutadiene–polyaniline core-shell microparticles. The significant variances of thermal conductivity and stiffness between rubber and conducting polymer revealed the remarkable responses in the microthermal analysis. The depth-dependent thermal microscopy controlled by the heating frequency distinguished the rubber core, which was buried under few micron thickness of polyaniline out layer. Local thermal analysis also demonstrated the heat penetration-dependent sensor response from the rigid polyaniline shell to soft polybutadiene core. These experimental results confirmed the core-shell structure of these microparticle materials, as well as the continuous conducting phase of polyaniline.

Keywords: Microthermal analysis; Scanning thermal microscopy; Core-shell; Polyaniline; Polybutadiene

1. Introduction

A Wollaston resistor type of micro thermal probe, acting simultaneously as a highly localized heat source and as a temperature sensor, has been developed and combined with atomic force microscopy (AFM), whereby the scanned thermal images and localized thermal analyses can be examined [1–3]. This technique named microthermal analysis (μTA^{TM}) has been widely applied to the characterizations of polymeric materials and pharmaceuticals [4,5]. Although no quantitative thermal signal can be obtained in this relatively new technology, its unique capability in collecting surface thermal properties on a micron scale does indeed provided valuable information.

In this research work, we demonstrate the application of microthermal analysis to the characterizations of polybutadiene–poly(sulfonated styrene)–polyaniline core-shell microparticles (PSSB–PANi), which were synthesized and reported elsewhere [6,7]. Hydroxy-terminated polybutadiene microparticles, 3–4 μm in diameter, were covalently bonded with different loadings of water-soluble poly(sulfonated styrene)–polyaniline (PSS–PANi) as the outer layers. These rubber-modified PSS–PANi complexes form stable and uniform aqueous latex formulations, even with a PANi loading of up to 58 wt.%. The electrical conductivity of these core-shell materials was found to be 0.1–1.0 S/cm, which is in the same magnitude

* Corresponding author. Present address: AST Products Inc., 9 Linnell Circle, Billerica, MA 01821, USA. Tel.: +1-978-957-6552; fax: +1-978-957-6552.
E-mail address: cskuo@attbi.com (C. Kuo).

0040-6031/03/$ – see front matter © 2003 Elsevier Science B.V. All rights reserved.
doi:10.1016/S0040-6031(03)00152-7

as that of PSS–PANi complexes without incorporated rubber components. According to optical microscopy results [7], the core-shell structures of PSSB4–PANi samples containing low PANi loading were not fully stable. The size of each microparticle in aqueous solution was dependent on the solution concentration, meaning that the low molecular weight PBD domains were able to aggregate due to their close proximity. However, with high PANi loading, such as sample PSSB4–PANi7, the size of these microparticles was found to be constant and independent of the solution concentrations. These observations had considerable effect on the ensuing microthermal analysis.

The significant variation of thermal conductivities and stiffness in the rubber and conducting polymer core-shell complexes on a micron scale provided an excellent model for an investigation of microthermal analysis. Local thermal analysis (LTA) has identified the thermal signal of rubber buried few microns below the surface. Scanning thermal microscopy (SThM) has also been used successfully for identification of high thermal conductivity domains, providing convincing evidence for a continuous conducting phase in this unique core-shell design. Alternating current (ac) thermal microscopy controlled by the heating frequency also demonstrated a capability for the depth-dependent thermal analysis.

2. Experimental

LTA, SThM, and topographic images were conducted using a model μTA^{TM} 2990 microthermal analyzer (TA Instruments Inc.) equipped with a Wollaston microthermal probe. The programmed temperature was calibrated using a poly(ethylene terephthalate) (PET) film at a heating rate of 25 °C/s. The onset melting point (260 °C) detected in the power curve was taken as the calibration temperature. Topographic images were recorded (through the *z*-axis piezo, Z-Piezo) with a force equivalent to 10 nA of sensor deflection. For SThM, the thermal conductivity mappings were collected based on the power required to maintain the probe at a given temperature. In the ac mode, the temperature modulation amplitude was ±3 °C with a frequency range from 1 to 20 kHz. Heat capacities were measured by temperature-modulated differential scanning calorimetry (TMDSC) in a DSC 2920 apparatus (TA Instruments Inc.) with a ±0.5 °C amplitude, 80 s period, and 4 °C/min heating rate. Results were further calibrated by using sapphire (Al_2O_3) as a standard. Studied materials were focused on PSSB4–PANi1 and PSSB4–PANi7 containing 16 and 58 wt.% of PANi, respectively. Sample films with thicknesses larger than 2 mm were used to avoid influences on the thermal signal by the substrates and boundaries. Single microparticles of PSSB4–PANi7 were prepared by casting dilute aqueous solutions onto a silicon wafer and drying at room temperature. A poly(methyl methacrylate) (PMMA) film containing SiO_2 microparticles was also investigated by temperature-modulated SThM. Opposite to the PSSB4–PANi samples, SiO_2/PMMA sample served as an example of microparticles with better thermal conductivity than the surrounded matrix. SiO_2 microparticles with 10–15 μm in diameter was first dispersed in a PMMA/THF solution, followed by solution casting on silicon wafer. After the solvent was evaporated, the film was peeled from silicon wafer and a smooth PMMA film with SiO_2 microparticles buried under the surface was obtained.

3. Results and discussion

3.1. Local thermal analysis on solid films of core-shell microparticles

Local thermal analysis in microthermal analysis reveals surface thermal responses within an area of only a few square microns. For non-homogeneous materials such as the core-shell microparticles, the localized thermal and mechanical responses can be examined and compared with the bulk properties. With the assistance of a surface mapping function, three locations on the film surface of PSSB4–PANi1 containing 16 wt.% of PANi were marked for the LTA measurements (see the inset in Fig. 1). The microscale surface bumpiness was caused by non-uniform shrinkage of PBD and PSS–PANi when the solid film was dried from its aqueous solution. Location 1 was directly above an aggregated rubber particle close to the surface. Its sensor response (curve 1 in Fig. 1) uncovered a “softening point” at about 225 °C. Because of the temperature gradient and dynamic thermal analysis in μTA measurement, the true softening temperature at location 1 was much lower than 225 °C.

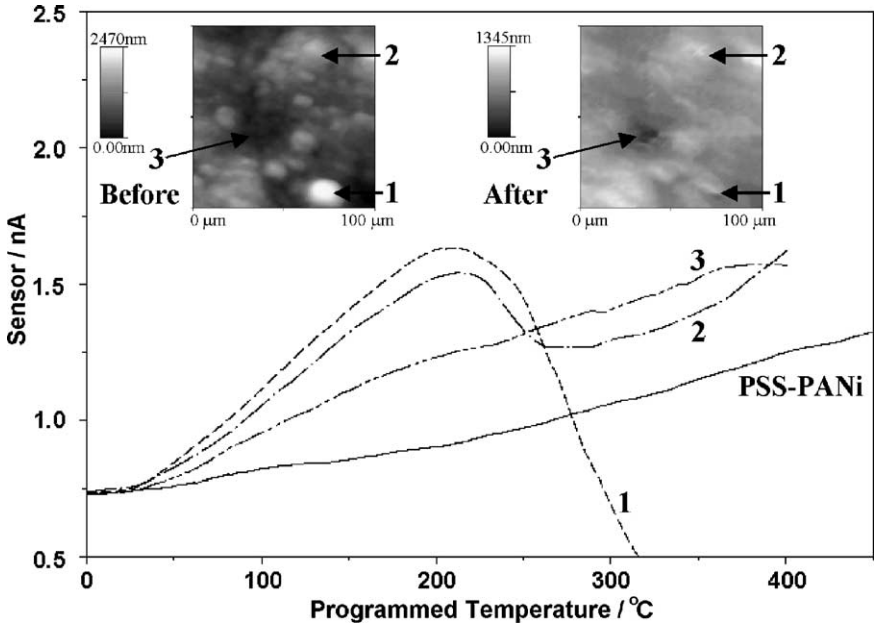

Fig. 1. Sensor responses of PSS–PANi and PSSB4–PANi1 with three selected locations as shown in the two inset topographic images before and after the three LTA measurements.

Compared with the data obtained by thermal mechanical analysis (TMA), the bulk softening temperature under the pressure of 455 kPa (66 psi) was about 45 °C [7]. As the microthermal probe was moved to location 3 where the surface morphology suggested no nearby rubber particles, no "softening point" was observed in the sensor signal. This sensor response was essentially similar to the PSS–PANi sample without rubber modification (also shown in Fig. 1). Interestingly, the same "softening temperature" observed at locations 1 and 2 suggested that a smaller rubber particle at location 2 was buried at the comparable depth as the bigger one at location 1, where the effective heat wave had extended at a similar rate.

The three "burn-marks" shown in the surface mapping after the three LTA measurements indicated that the outer layer containing low PANi-loading had failed to protect the rubber core in the case of the PSSB4–PANi1 sample containing 16 wt.% of PANi. The PBD core had melted, and the probe pushed and sunk slightly into the material surface. As a result, the increase of contact area between the probe and sample surface encouraged more heat transfer and showed endothermal-like features in the power profiles (Fig. 2). It was more evident in the first derivative of power (see the inset). Because of this contact area change, apparently these signals were not the true thermal responses of PSSB4–PANi core-shell microparticle.

As to the solid film of sample PSSB4–PANi7 containing 58 wt.% of PANi, the rigid shell has fully

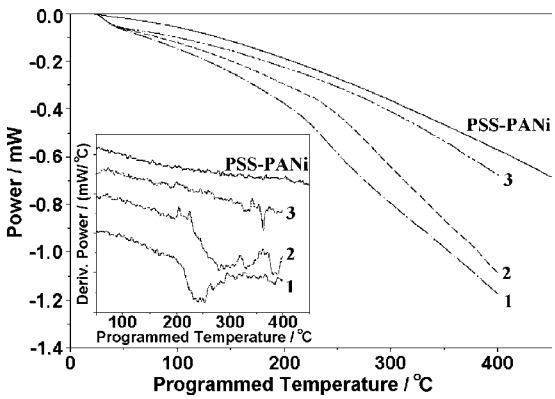

Fig. 2. Power profiles of PSS–PANi and PSSB4–PANi1 with three selected locations as shown in Fig. 1. The inset is the first derivative of power profiles.

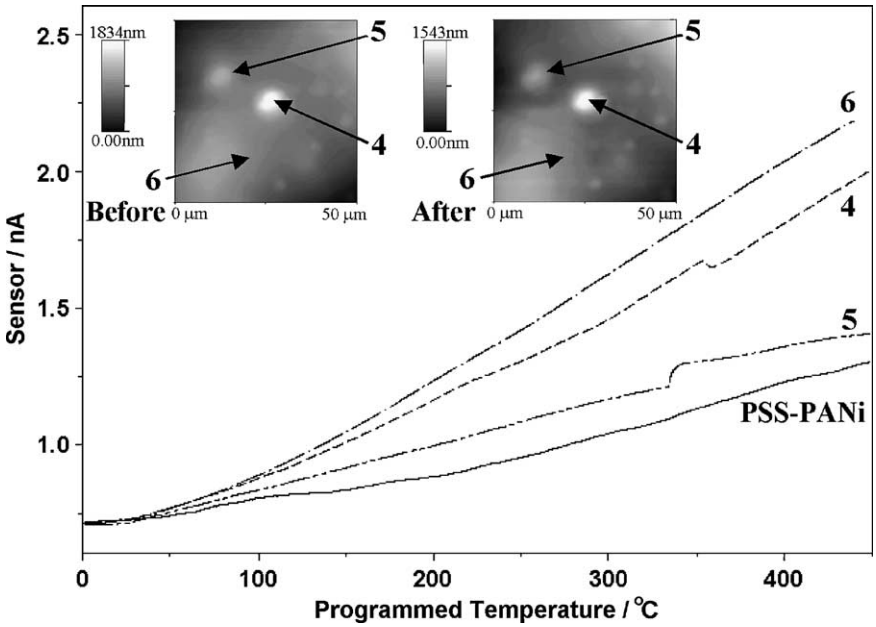

Fig. 3. Sensor responses of PSS–PANi and PSSB4–PANi7 with three selected locations as shown in the two inset topographic images before and after the three LTA measurements.

covered the soft rubber core, as evidenced by the constant particle size observed in the optical microscopy [7]. In the sensor responses examined by procedures similar to the previous case, the continuous and steady volume expansion with increasing temperature was almost the same as that of the PSS–PANi sample (Fig. 3). The soft rubber segment did not contribute much in the way of mechanical property in the micron scale at given temperature ranges. However, the heat transfer (the power curve) at location 4 shown in Fig. 4 slightly increased at about 225 °C, indicating a possible melting of rubber phase, and was soon followed by a rapid energy recovery at 280 °C. The first derivative power curve thus showed a broad endothermic peak and a sharp exothermal-like peak. Because no sudden sensor signal was recorded at this temperature and no "burn-mark" was found afterward, potential mechanical interferences and significant contact area variation were eliminated. One explanation for this unusual exothermal-like response is that the energy regain recognized from a slowing-down of the heat transfer as the heat wave reached the low thermal conductive PBD phase. It is important to clarify that the power derivative curve in microthermal analysis commonly used for identification of endo- and exothermic events does not have the same physical meaning as those encountered in conventional DSC analysis. In fact, the power derivative with units of mW/s (or mW/°C) represents the acceleration of heat transfer, and is

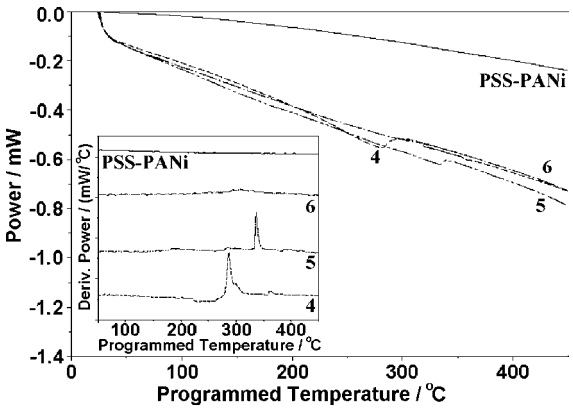

Fig. 4. Power profiles of PSS–PANi and PSSB4–PANi7 with three selected locations as shown in Fig. 1. The inset is the first derivative of power profiles.

not necessary to be an energy absorption ($-\Delta H$) or an energy release ($+\Delta H$) from samples. The sharp exothermal-like response shown at location 5 (in Fig. 4) and corresponding quick change in sensor signal suggested the movement of the thermal probe during the measurement. No sensor or thermal change was picked up at location 6.

3.2. Local thermal analysis on core-shell single microparticle

Based on the thermal analyses of the solid film surfaces, an investigation on single core-shell microparticles was encouraged. Individual microparticles of PSSB4–PANi7 were prepared by casting dilute aqueous suspensions on a silicon wafers. The silicon wafer substrate provides a smooth surface where microparticles can be distinguished easily with SThM. It also has higher thermal conductivity in comparison with the polymeric materials, allowing easy distinctions in the power signals, to make sure that the 2 μm diameter thermal probe has precisely targeted on a core-shell particle with diameter of only 4–5 μm. If the thermal probe missed the microparticle target, either the probe movement was pick up in sensor signal or power signal showed a much fast heat transfer. Surface mapping was carried out first in order to locate the microparticles. In Fig. 5, a single PSSB–PANi7 microparticle was identified and checked three times LTA measurements directly at the particle center. The sensor responses showed a reproducible softening temperature between 350 and 420 °C. Gradually reduced softening temperatures suggested an orientation of PBD molecular chains after the heat treatments. More excitingly, the particle morphology remained the same as shown in the second mapping images after the three LTA measurements. These results confirmed the complete core-shell structures, in which the PBD rubber was protected by a PSS–PANi shell even at temperatures near 450 °C. It also demonstrated existence of a conducting rubber microparticles with elastic performance.

3.3. Heat capacity and thermal conductivity measurements

The heat capacities were determined by temperature modulated differential scanning calorimetry

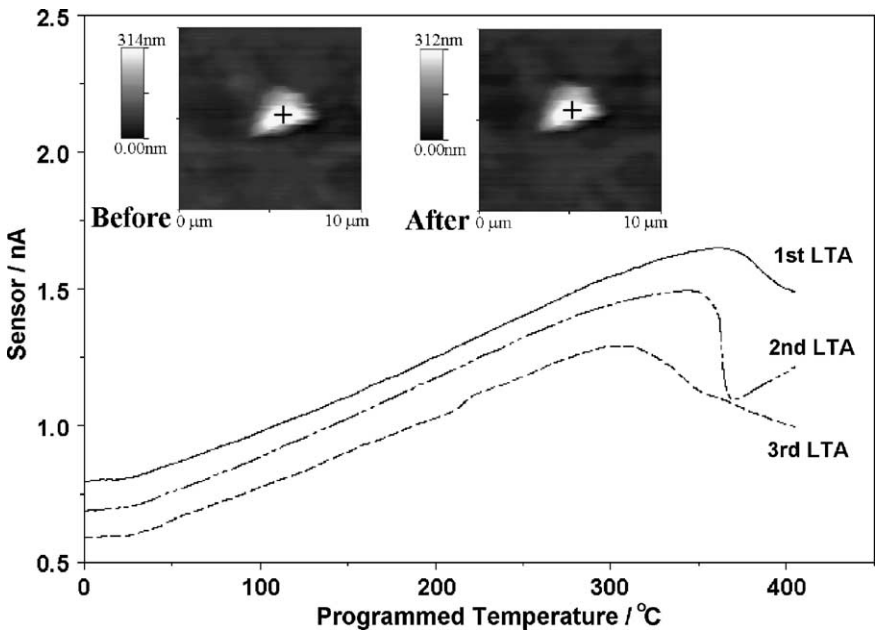

Fig. 5. Sensor responses of three LTA measurements on a single microparticle of PSSB–PANi7. Two insets show the topographic images before and after the three LTA measurements.

(TM-DSC) with measuring conditions of ±0.5 °C amplitude, 80 s period, and 4 °C/min heating rate. These results were further calibrated by using sapphire (Al_2O_3) as a standard. Data shown in Fig. 6 are the second measurements for each sample to avoid interference from residual moisture. The heat capacity curves of PSS–PANi and PSSB4 are located between those of the two starting materials of HT-PBD and PSS. It can be seen that the heat capacity profiles of PSSB4 and PSS–PANi are very close, with no significant difference in the values for samples of PSSB4–PANi1 and PSSB4–PANi7. The heat capacity of pure polyaniline powder does seem to be out of the ordinary above 110 °C. This is believed to be due to deficient heat transfer in the powder sample, this being a critical factor in TM-DSC measurements. It was also found in Fig. 6 that the heat capacity of HT-PBD was about 30% higher than that of PSS–PANi. In terms of thermal stability, the rubber core therefore was able to absorb more heat and still physically retain the same shape because of the protective shell. In other words, the HT-PBD core and the PSS–PANi shell both had enhanced thermal stability in different ways. Heat capacity data will be further used and analyzed for the modeling and calculations in the microthermal analyses.

The application of microthermal analysis to quantitative thermal analysis of material surfaces has been investigated only very recently [8–10]. Although there are some uncertain factors in terms of modeling and experimental approaches, the surface thermal conductivity measured by microthermal analysis still provides satisfactory accuracy. In theory, the direct current (dc) power required to maintain the thermal probe at a given temperature or temperature profile is highly dependent on the thermal conductivity near the sensor. Several research groups have developed modeling and heat equations for the resistive thermal sensor under either direct current or modulated current modes [11–13]. For low thermal conductivity materials, such as polymers, the heat equation can be simplified as $2\pi k_s b\theta_p$ [11], meaning that the power is only a function of thermal conductivity (k_s), contact size (b, the probe radius), and the probe temperature (θ_p). Probe temperature (θ_p) is controlled during the measurement, and the contact size (b) is assumed to be a constant under the conditions of using the same probe and appropriate temperature range without any physical change in the materials. Therefore, the surface thermal conductivity (k_s) can be obtained using only the calibration data from several standard samples with similar thermal conductivities.

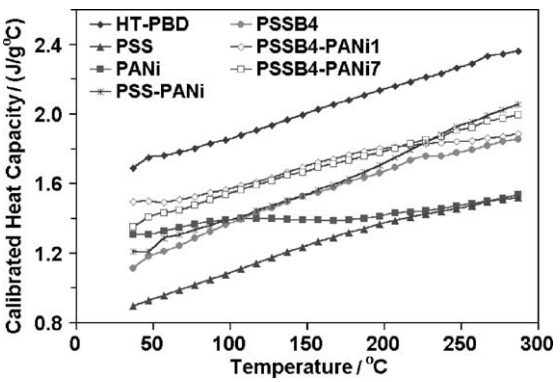

Fig. 6. Heat capacities of HT-PBD, PSS, PANi and PSSB–PANi complexes measured by temperature-modulated DSC.

In our investigations, polymeric materials, including polystyrene (PS), polypropylene (PP), poly(ethylene terephthalate) (PET), poly(vinyl chloride) (PVC), and high-density polyethylene (HDPE), were employed as standard samples to establish the thermal conductivity calibration curve. Glass was also used as a higher thermal conductivity specimen. LTA data were recorded at least five times for each sample with testing temperature ranging from room temperature to 100 °C. Within this temperature range, no physical changes were recorded or expected from the standard samples and the core-shell polyaniline materials. Note that a smooth surface for each testing sample is required in order to minimize errors arising from the contact size. As the slope of the straight power curve varied between 60 and 100 °C, the first derivative power (mW/K), was plotted versus the correlated thermal conductivities. An excellent calibration curve as shown in Fig. 7 was obtained. In the low thermal conductivity range, the standard samples showed a linear relationship, as would be expected from the heat equation. However, due to a higher thermal conductivity from PANi-containing samples, an exponential calibration curve was established, so that the data point for glass could also be covered. The liquid low molecular weight HT-PBD sample could not be examined by the same method. Its data point in Fig. 7 was obtained from the supplier. PSS–PANi sample

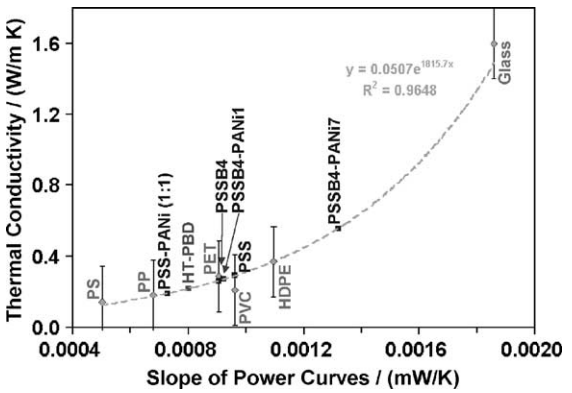

Fig. 7. The thermal conductivity calibration curve obtained by the slopes of power profiles between 60 and 100 °C.

without rubber modification showed a lower thermal conductivity than expected was due to its preparation by powder sample compression. Other calibrated thermal conductivities of PSS, PSSB4, and two PSSB4–PANi samples are summarized in Table 1. Interestingly, the thermal conductivity of PSSB4 was located between the corresponding values for PSS and HT-PBD, with a linear interpolation of about 80:20, the same as its component ratio. As the PANi moiety was introduced, thermal conductivities of PSSB4–PANi samples also climbed up to 0.5582 W/m K, more than twice as high as the value of PSSB4.

3.4. Scanning thermal microscopy

Microthermal analysis has often been utilized for surface morphology studies, especially on heterogeneous materials containing two or more different components [14,15]. Scanning thermal microscopy records thermal conductivity information by monitoring the power required to maintain the thermal probe at a given temperature while doing the surface mapping. Materials with good thermal conductivity tend to "consume" more energy from the thermal probe, due to better heat transfer. Low thermal conductivity materials, in contrast, perform more like insulators, and claim less energy from the probe. As a result, thermal conductivity can be recorded and distinguished for each component, even if it is a few microns below the surface. Fig. 8 shows an example of thermal mapping for a PSSB4–PANi1 solid film, with data collected with the probe temperatures at 30, 80 and 240 °C. Although the surface morphology and sensor responses remained the same when the probe temperature was increased to more than 200 °C, the thermal conductivity images were indeed enhanced by the high temperature probe. The white area in thermal conductivity images corresponds to the PSS–PANi domain, and the darker region corresponds to PBD. As mentioned earlier, the PBD phase in this low PSS–PANi loading sample was able to aggregate and form larger particles with size even up to 20 μm. Nevertheless, the high thermal conductivity regions indicated a continuous

Table 1
Heat capacity and thermal conductivity

Sample	Specific gravity (ρ)	Heat capacity (Cp) (J/g K)[a]	Thermal conductivity (ref.) (k) (W/m K)	Thermal conductivity (cal.) (k) (W/m K)	Thermal diffusivity (D) (m^2/s)
PS[b]			0.1420	–	
PP[b]			0.1800	–	
PET[b]			0.2884	–	
PVC[b]			0.1800	–	
HDPE[b]			0.3700	–	
Glass[b]			1.6000	–	
HT-PBD	0.901	1.8528	0.2170	–	1.29×10^{-7}
PSS	1.40	1.0792	–	0.2907	1.92×10^{-7}
PSSB4	1.30	1.3621	–	0.2622	1.48×10^{-7}
PSSB4–PANi1	1.32	1.5638	–	0.2710	1.31×10^{-7}
PSSB4–PANi7	1.36	1.5351	–	0.5582	2.67×10^{-7}
PSS–PANi (1:1)	1.40	1.3870	–	0.1904	0.98×10^{-7}

[a] Heat capacity at 100 °C measured by TM-DSC.
[b] Standard.

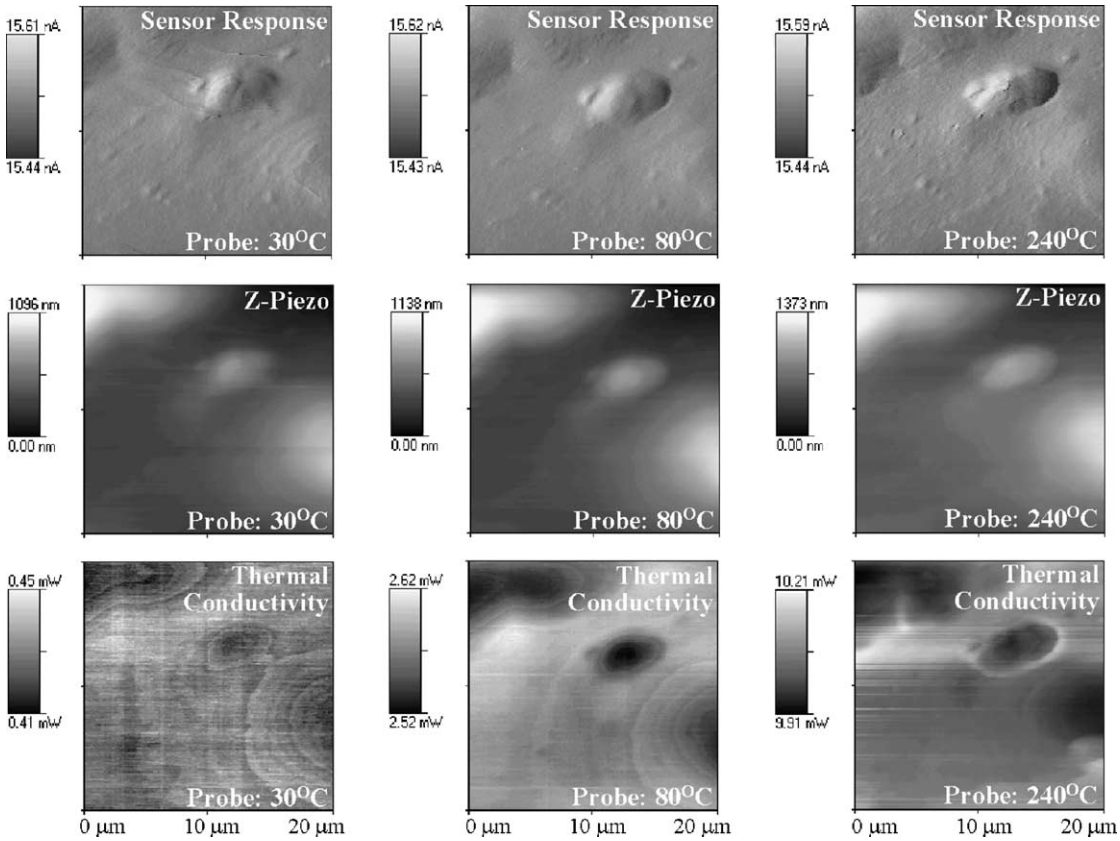

Fig. 8. Sensor response, topographic (Z-Piezo) and thermal conductivity images (20 μm × 20 μm) of PSSB4–PANi1 solid films under the probe temperatures at 30, 80 and 240 °C.

PDD–PANi phase surrounding the PBD particles. For comparison, a PSS–PANi sample without PBD loading was also examined under the same conditions. As expected, the results did not indicate much morphology or thermal conductivity tolerance. In the case of PSSB4–PANi7, the PSS–PANi apparently dominated the thermal conductivity mapping as shown in Fig. 9. PBD particles (the dark spots) with maximum diameters of 5 μm also matched the signal core-shell size observed in optical microscopy. With this thermal conductivity morphology, there was no doubt that the PSS–PANi phase in PSSB4–PANi7 was continuous.

3.5. Temperature modulated microthermal analysis

The most interesting demonstration in microthermal analysis involves the applications of ac mode and modulated temperature control, where direct current is replaced by the alternating current. Due to the size of thermal probe and heating area, heating and cooling rates estimated in the range of a few tens of nanoseconds [16] are fast enough to perform a complete ac cycle. Theoretically, the temperature distribution under a temperature-modulated heat source can be expressed as $T = T_0 \exp(-L/L_0)$, where T_0 is the probe temperature and L is the depth below the surface. The thermal diffusion length, $L_0 = (D/\omega)^{1/2}$, is a function of the thermal diffusivity (D) of the material and the angular frequency of modulation (ω). In general, the effective diffusion length (d) is considered to be the penetration depth where the temperature increases can reach half of the surface temperature (T_0). The mathematical expression of d then becomes $d \cong (2D/\omega)^{1/2}$. For most common polymeric materials, the heat penetration depth (d) is in the range of few microns in the ac frequencies from 1 to 50 kHz.

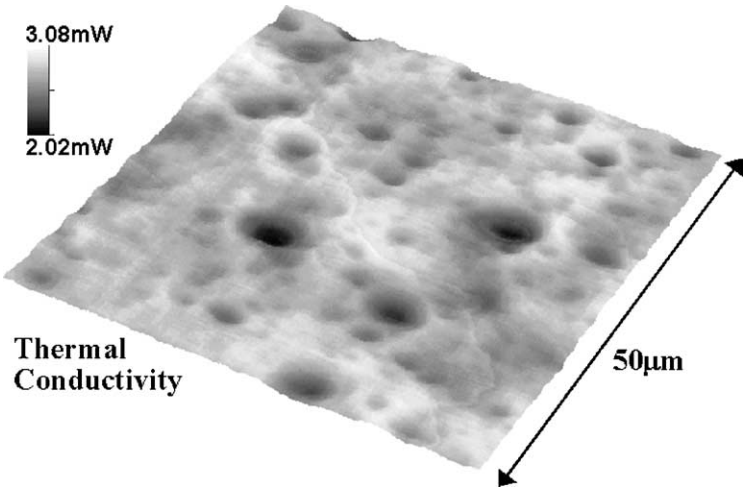

Fig. 9. Thermal conductivity mapping of PSSB–PANi7. Bright area is PSS–PANi domain, and the dark spots represent the PBD cores.

In reality, however, the three-dimensional thermal wave with modulated temperature is expressed and projected into two-dimensional surface mapping. Frequency-dependent depth of heat penetration based on one-dimensional heat transfer is too much of a simplification, in addition to the fact that the gradient temperature distribution under the heat source makes it difficult to define the real distance of the effective heat transfer. Several research groups, therefore, have proposed more complex modeling systems for SThM in an ac mode. For example, the thermal probe can be still simplified as a one-dimensional thermal couple, and the three-dimensional heat transfer between probe and material surface can be estimated [17–19]. Second (2ω) and third harmonic signals (3ω) have also been investigated as a possible means to produce thermal images in three-dimensions [20].

Before ac SThM measurements on PSSB4–PANi samples were experimentally investigated, their thermal diffusivities (D) were first calculated based on the equation, $D = k/\rho Cp$, where k, ρ and Cp are the thermal conductivity, density and heat capacity, respectively. Thermal conductivities were measured as discussed previously. Heat capacities at 100 °C obtained in TM-DSC were employed because it is the same probe temperature used in the ac SThM. Results of these thermal parameters are summarized in Table 1.

Fig. 10 shows an example of a PSSB4–PANi7 solid film examined using ac SThM. The probe temperature was maintained at 100 °C with a temperature amplitude of ±3 °C and ac frequencies varied from 1 to 20 kHz. Since the temperature was kept constant in the SThM, the probe resistance was also unchanged. Therefore, the temperature-modulated amplitude recorded as a voltage is directly proportional to the square root of power, and provides the same information as that obtained in thermal conductivity mapping, i.e. the power required to maintain the probe temperature. In the modulated amplitude image shown in Fig. 10, a PBD particle of 4 μm in diameter was identified and its thermal morphologies were shown to be ac-frequency dependent. The amplitude readings at the area away from any PBD particles in the line measurements are considered as the constant baseline, so that the differential amplitude readings at the PBD particle location can be exported and analyzed. The dramatic amplitude drop located at the rubber particle, especially at low ac frequency, indicated that the low thermal conductive PBD microparticle has preserved a certain amount of heat transfer. At low frequency, the heat wave penetrated more deeply and accumulated more contribution from PBD domain.

In order to obtain a better understanding of the ac SThM results, a simple model as shown in Fig. 11 was further investigated using a single PBD micro-sphere of 4 μm in diameter located 2 μm below the surface. The volume and the volume percentage of PBD and PSS–PANi domains were first revealed as a function

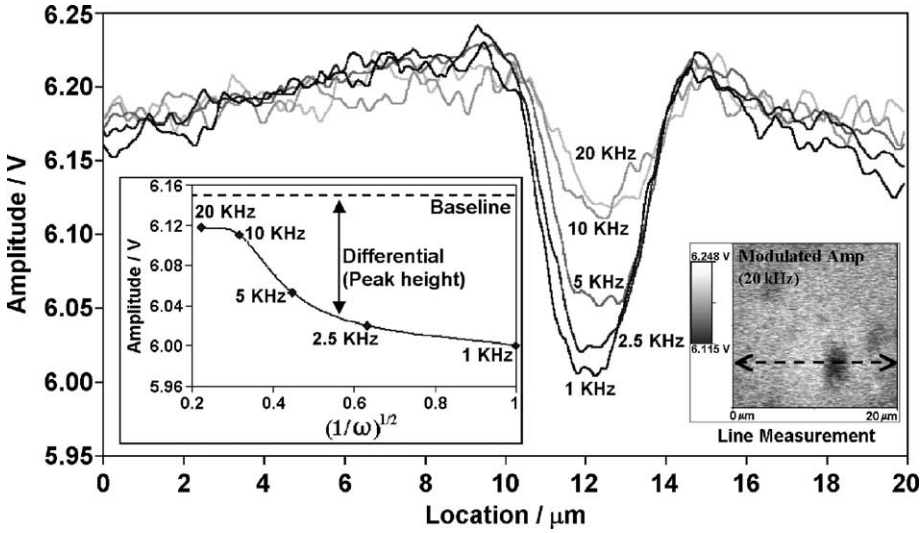

Fig. 10. Temperature-modulated SThM of PSSB4–PANi7 solid film by the ac frequencies as indicated. The probe temperature is 100 °C with ±3 °C amplitude. The line measurements crossed the near-surface PBD particle are exported and analyzed. The inset shows the amplitude vs. the function of $(1/\omega)^{1/2}$. Baseline represents the amplitude at the area without PBD domain.

of the distance from the heat source. Although the PBD domain has reached only a maximum of 12 vol.%, its contribution in the total heat transfer will still intensify the differential of the heat dissipation. The frequency-dependent temperature distributions under a temperature-modulated heat source at 100 °C were calculated according to the heat equations mentioned previously. Then, the total heat consumption for this modeling systems of a PBD micro-sphere located 2 μm below the surface can be estimated and subtracted from the same heat consumption of the model without a PBD micro-sphere. In Fig. 12, the experimental amplitude square curve (V^2) proportionally matches with the modeling profile. The major

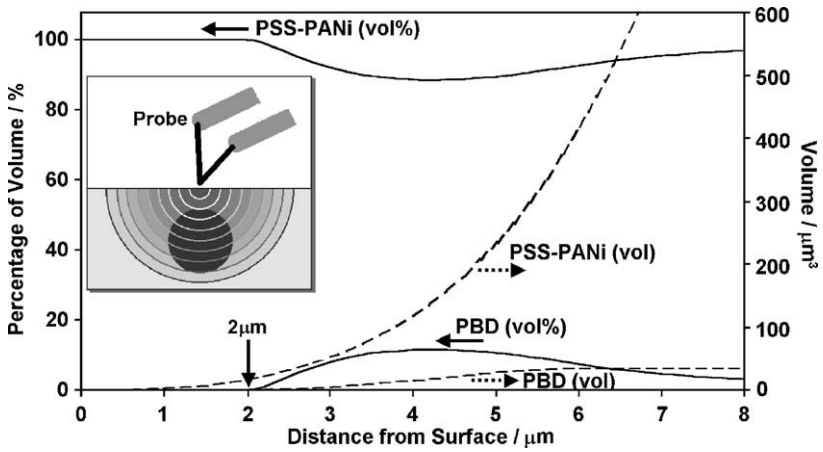

Fig. 11. The inset shows a model of single PBD micro-sphere of 4 μm in diameter located 2 μm below the surface for the accountable volume to ac heat wave. Dash curves represent the volumes of PBD core and PSS–PANi shell within the half sphere territory; solid curves are the volume percentages of PBD core and PSS–PANi shell.

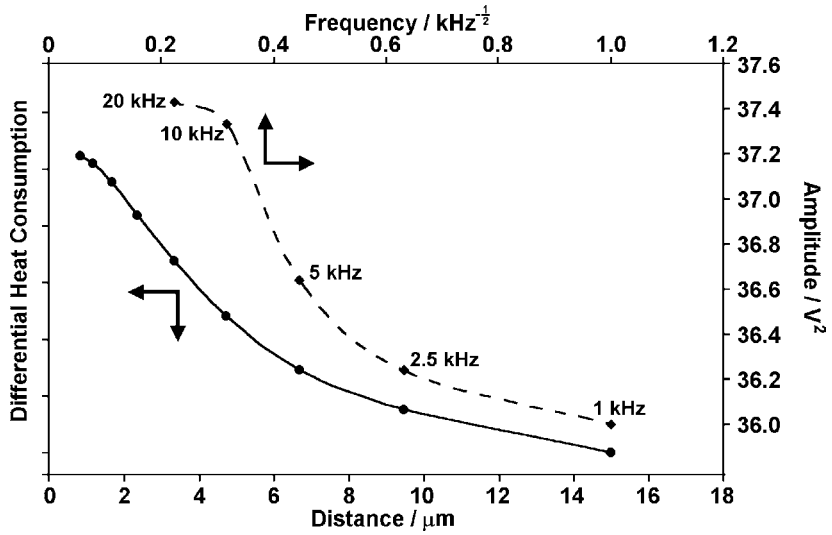

Fig. 12. Dash curve represents the square of amplitude (proportional to power) vs. ac frequencies ($(1/\omega)^{1/2}$). The solid curve is the differential heat consumption as a function of heat penetration depth, calculated by a model of a PBD micro-sphere of 4 μm in diameter located 2 μm below the surface.

variation at low heat penetration range (or high ac frequency) was presumably caused by the surface cooling and the movement of the scanning thermal probe. Also, the effective diffusion length calculated in the modeling system was based on the thermal properties of PSSB–PANi matrix, which was not appropriate as the heat wave reaches the low conductive PBD phase.

For low PANi loading samples, such as in the case of PSSB4–PANi1, the difference of thermal properties between rubber and conducting polymer domains is much less significant. Meanwhile, PBD cores gather too closely to separate their thermal responses. The heat wave always penetrates and covers more than one core-shell microparticle. Consequently, the temperature-modulated thermal profiles as a function of heat penetration depth lose their sensitivities in the surface mapping images.

In a separate experiment, similar ac microthermal analysis was performed on a PMMA film containing SiO_2 microparticles. Because SiO_2 is a better conductor than PMMA, the ac thermal mapping shown in the inset of Fig. 13 recognizes the particles as bright spots, opposite to the PBD cores in the PSSB4–PANi7 sample. The line measurements of modulated amplitude mappings, therefore, give upward profiles representing the locations of three SiO_2 particles. In this case, the frequency-dependent thermal response was also observed.

Fig. 14 summarizes the two temperature-modulated SThM models for the non-homogeneous materials containing either good or poor conductive microparticles, compared to their surrounded matrixes. For the homogeneous samples (curves a2 and b2), the frequency-dependent heat transfer climbs first as more material covered by the hemispheric heat penetration range, then it gradually saturates to an equilibrium that presumably is the same heat transfer as the isothermal treatment. In the case of materials containing poor conductive cores as the second phase, like PBD microparticles in PSSB–PANi7, the reduced heat transfer was expected inside the PBD domain. As a result, the differential heat transfer between the locations with and without PBD phase was less at the high ac frequency heating (curve a3 in Fig. 14). Once the heat wave effectively covered the whole microparticle at low ac frequency heating, the differential heat transfer was enlarged and stabilized. For the opposite case, a SiO_2 particle with better thermal conductivity than the matrix speeded up the heat transfer inside the core and expanded the differential heat transfer at the high ac frequency heating. Curve b3 shown in Fig. 14 is about

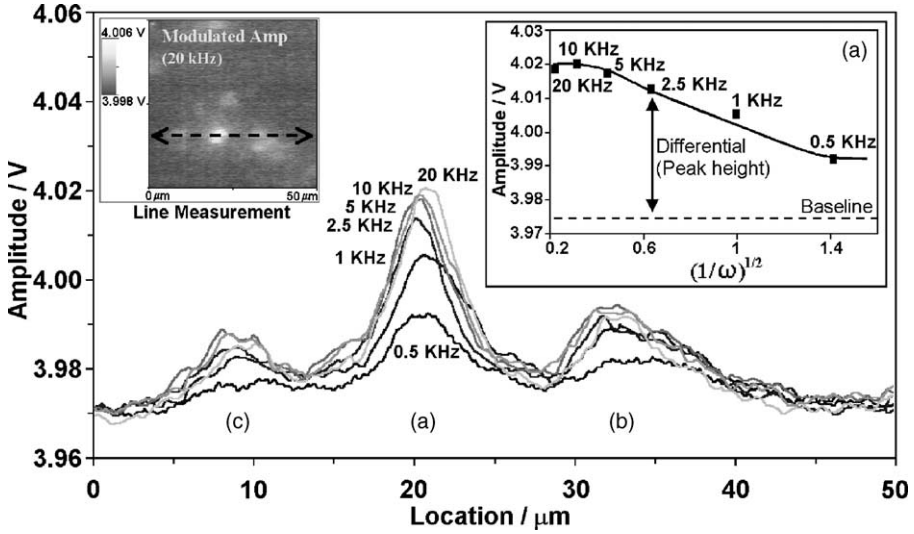

Fig. 13. Temperature-modulated SThM of SiO_2/PMMA solid film by the ac frequencies as indicated. The probe temperature is 80 °C with ±3 °C amplitude. The line measurements crossed the near-surface SiO_2 particles, labeled as (a), (b) and (c), are exported and analyzed. The inset shows the amplitude vs. the function of $(1/\omega)^{1/2}$. Baseline represents the amplitude at the area with SiO_2 domain.

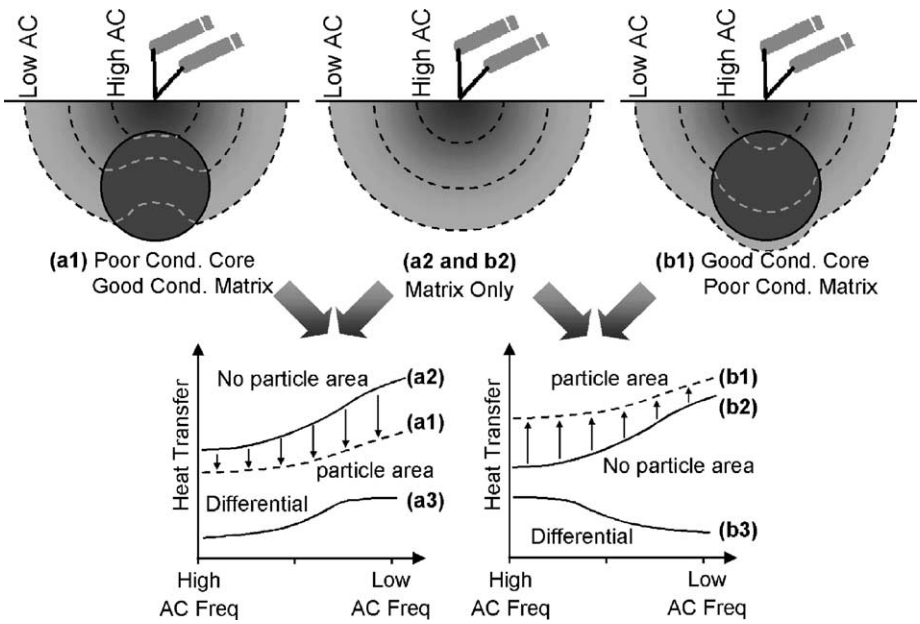

Fig. 14. Comparison of good and poor conductive cores in the temperature-modulated SThM as a function of ac frequencies. Curves a2 and b2 are ac frequency-dependent heat transfer of good and poor conductive matrixes. Curves a1 and b1 represent the heat transfer at the locations of poor and good conductive particles. Curves a3 and b3 are the differential heat transfers at both cases.

a mirror profile to curve a3. These observations suggest the different strategies to the morphology investigation in temperature-modulated SThM. For good conductive subjects hidden under the surfaces, high ac frequency heating can enhance the morphological images. Lower ac frequency heating is recommended to capture the poor conductive objects below the surfaces.

4. Conclusions

Microthermal analysis has proven to be an excellent technology for the investigation of non-homogeneous materials, such as core-shell polyaniline microparticles. Local thermal analysis revealed localized thermal responses in a few square microns of area, and discerned the mechanical properties of the rigid PANi shell from those of the soft PBD core. Scanning thermal microscopy collected surface thermal information and confirmed the presence of continuous conducting phase in these unique core-shell approaches. Modulated microthermal analysis also demonstrated the frequency-dependent thermal properties and the depth-dependent morphology of the core-shell polyaniline microparticles.

Acknowledgements

The authors thank Dr. Mario Cazeca of AST Products Inc. for his helpful discussion and Dr. Gray Slough of TA Instruments Inc. for the valuable support on the μTA™ instrument.

References

[1] A. Hammiche, M. Reading, H.M. Pollock, M. Song, D.J. Hourston, Rev. Sci. Instrum. 67 (1996) 4268.
[2] D.M. Price, M. Reading, T.J. Lever, J. Therm. Anal. Calorim. 56 (1999) 673.
[3] M. Reading, D.M. Price, H.M. Pollock, A. Hammiche, A. Murray, Am. Lab. 31 (1999) 13.
[4] M. Reading, D.M. Pricel, D. Grandy, H.M. Pollock, A. Hammiche, Polym. Prepr. 41 (2000) 1418.
[5] D.Q.M. Craig, V.L. Kett, C.S. Andrews, P.G. Royall, J. Pharm. Sci. 91 (2002) 1201.
[6] C. Kuo, L.Y. Chiang, J. Kumar, L. Samuelson, S.K. Tripathy, Polym. Prepr. 41 (2000) 1768.
[7] C. Kuo, L. Samuelson, S.P. McCarthy, S.K. Tripathy, J. Kumar, J. Macromol. Sci. A: Pure Appl. Chem., 2003, in press.
[8] F. Ruiz, W.D. Sun, F.H. Pollak, C. Venkatraman, Appl. Phys. Lett. 73 (1998) 1802.
[9] G.B.M. Fiege, A. Altes, R. Heiderhoff, L.J. Balk, J. Phys. D: Appl. Phys. 32 (1999) L13.
[10] A.I. Buzin, P. Kamasa, M. Pyda, B. Wunderlich, Thermochim. Acta 381 (2002) 9.
[11] A. Majumdar, Annu. Rev. Mater. Sci. 29 (1999) 505.
[12] I. Moon, R. Androsch, W. Chen, B. Wunderlich, J. Therm. Anal. Calorim. 59 (2000) 187.
[13] V.V. Gorbunov, N. Fuchigami, V.V. Tsukruk, Probe Microsc. 2 (2000) 53.
[14] E. Gmelin, R. Fischer, R. Stitzinger, Thermochim. Acta 310 (1998) 1.
[15] V.V. Gorbunov, N. Fuchigami, J.L. Hazel, V.V. Tsukruk, Langmuir 15 (1999) 8340.
[16] H.M. Pollock, A. Hammiche, J. Phys. D: Appl. Phys. 34 (2001) R23.
[17] F. Depasse, S. Gomes, N. Trannoy, P. Grossel, J. Phys. D: Appl. Phys. 30 (1997) 3279.
[18] S. Gomes, F. Depasse, P. Grossel, J. Phys. D: Appl. Phys. 31 (1998) 2377.
[19] S. Gomes, N. Trannoy, F. Depasse, P. Grossel, Int. J. Therm. Sci. 39 (2000) 526.
[20] R. Smallwood, P. Metherall, D. Hose, M. Delves, H. Pollock, A. Hammiche, C. Hodges, V. Mathot, P. Willcocks, Thermochim. Acta 385 (2002) 19.